Utrecht University
and
Bijvoet Center for Biomolecular Research
NMR Spectroscopy Research Group

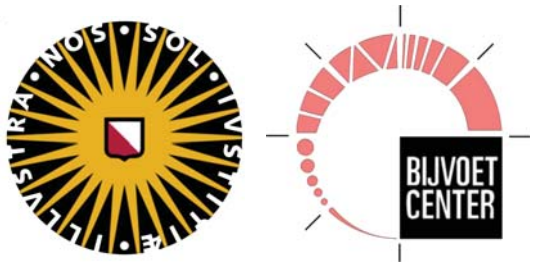

Report

"On the Molecular Determinants of Modal Gating Shifts in Potassium Channels"

Major Internship from

October 2017 to October 2018

Felix Kümmerer
6261485

Molecular and Cellular Life Sciences

Supervisor: Dr. Markus Weingarth

Second Reviewer: Prof. Dr. Alexandre Bonvin

Utrecht 2018

Table of contents

1 Laymen's summary

Knowing the structure of a protein is extremely useful to understand its function. However, in the last years it was emerging that it is not enough to know the structure of a protein, but that dynamics of a protein are crucial for its function. In proteins, dynamics can occur on different time-scales and levels, such as motions of the whole protein or just of some local regions of the protein. Understanding these motions can therefore help to elucidate important functional properties of a protein. This information can then, for instance, be used in drug development to target malfunctioning proteins which are often the basis for diseases.

One type of such relevant proteins are ion channels, which form pores in cellular membranes to regulate the flux of electrically charged atoms or molecules (ions), through the membrane. Accumulation of these ions can then lead to a build-up of an electrochemical gradient along the membrane, which is essential for many cellular tasks, such as signalling across these cells and muscle contraction. In humans, malfunctioning of ion channels can cause various diseases, such as cardiac arrhythmia or neuronal diseases.

Potassium (K^+) is a positively charged ion and it is one of the most important ions in the cell, where it is part of a variety of physiological processes. The transport of K^+ is mediated by so-called K^+ channels and their activity is believed to be regulated by a complex interaction-network within the channel-pore (gating). KcsA is a bacterial K^+ channel of which the setup of functionally important regions, such as the pore forming selectivity filter, are very similar to eukaryotic K^+ channels, making it a well-accepted model to study potassium channels. For many ion channels it was shown, that the channel can shift between different activity modes allowing fine regulation of the ion flux (modal gating). If a specific amino acid in the selectivity filter of KcsA is replaced by another one, the channel gets locked in different gating modes, making these mutants perfect models to investigate modal gating shifts.

Studying internal dynamics can help to gain a better understanding of this mechanism. However, it is challenging to study these dynamics because they are highly dependent on external conditions, such as temperature or the chemical environment. Therefore, it is desirable to work at conditions that are as close as possible to the natural environment of these proteins. Solid-state nuclear magnetic resonance spectroscopy (ssNMR) is a technique that is uniquely suited to study these protein dynamics at near-native conditions and physiological temperatures.

Our ssNMR studies on KcsA show that the mutations, which are representative for different gating modes, cause conformational changes in the pore-forming selectivity filter of the channel and its surroundings. Investigating the dynamics demonstrated that the mutant channels display distinct motional landscapes with marked differences in the selectivity filter, which can trigger modal gating shifts. This study gives high-resolution information about the key determinants and mechanisms of modal gating in K^+ channels.

2 Abstract

Modal gating describes the shifting between different gating modes in ion channels, which is believed to be a widespread mechanism for the control of ion conductance. The K^+ channel KcsA can shift into distinct, and under stable experimental conditions stochastically occurring, gating modes. Presumably, this is regulated by a water and hydrogen-bonding network behind the selectivity filter, but the molecular determinants are still unclear. Point mutations in this hydrogen-bond network of KcsA can lock the ion channel into one the natively occurring gating modes, making them a good model to study these modal gating shifts.

Here, we use advanced ^{1}H-detected solid-state NMR at native-like conditions to elucidate the origin and molecular determinants of these modal gating shifts. We show that E71X mutations, which are representative for these different gating modes, cause stark conformational and motional changes of the selectivity filter and its surroundings. This results in rearrangements of the hydrogen-bond and water network behind the selectivity filter, indicating that these distinct conformational dynamics of the selectivity filter trigger modal gating shifts. Furthermore, we demonstrate marked changes in the conformational and motional landscape of the selectivity filter, providing a foundation on a molecular level for the better understanding of eukaryotic K^+ channels.

3 Introduction

3.1 Membrane Proteins and how to study them

Membrane proteins make up 20 to 30% of the proteomes of most organisms.[1] A large group of these proteins form integral channels or pores and mediate the transport of molecules and ions through the membrane. Ion channels are fundamental components of excitable cells and they control the flux of ions through the membrane. This results in an electrochemical gradient along the membrane which is essential for signalling across these cells and their functions, such as muscle contraction or hormone secretion.[2]

The function and importance of ion channels and transporters make them a popular target for pharmaceuticals, resulting in intensive research on them. However, studying these membrane proteins presents challenges.[3] Unlike soluble proteins, membrane proteins require not only the right buffer, but also the presence of a lipid membrane which ensures the correct fold and structure of the proteins. To a certain extent, this can be mimicked by using detergents that form micelles under aqueous conditions, and thus offering the proteins a matrix that can stabilize their structure and protect the hydrophobic intermembrane components from the hydrophilic buffer environment.[4,5] Natural lipid membranes, however, contain a mix of numerous different lipids and other components, such as sterols, glycolipids or -proteins and of course other proteins that influence the structure, stability and function of membrane proteins.[6,7] Research of membrane proteins requires elaborate sample preparation. Hence, structure determination is difficult using techniques such as solution state nuclear magnetic resonance (NMR) or X-ray diffraction. Using solution state NMR is only possible to a certain extent (only in micelles, detergents and potentially in nanodiscs, but not liposomes) and is limited to the size of the proteins and the slower overall tumbling of large membranes. Crystallization of a membrane protein usually requires the use of detergents, antibodies or other non-native additives which might influence the structure and function of the protein of interest. Cryo-electron microscopy (EM) and tomography overcome some of these problems and play an increasingly important role for structural studies of proteins or protein complexes.[8]

However, it is not enough to have high-resolution structures and models available to understand the function of proteins and their domains. Information about internal and global dynamics of the protein are crucial to understand their function.[9] Both, X-ray diffraction and Cryo-EM display a static snapshot of the protein as it is crystallized or cryogenically frozen and therefore do not inform on motional timescales. In contrast, NMR can give information about structural components as well as protein dynamics on several timescales. Modern proton-detected (^{1}H-detected) solid state NMR (ssNMR) experiments at high magic angle spinning (MAS) frequencies allow to study proteins or complexes that are too large for solution-state NMR with a good sensitivity and high resolution.

Furthermore, it is possible to perform ssNMR experiments at native-like conditions, using lipid membranes, physiological temperatures and buffer conditions.

3.2 Introduction to Potassium Channels and Modal Gating

KcsA is a pH-gated potassium channel from the bacteria *Streptomyces lividans* and like all potassium (K^+) channels, it enables rapid and a highly selective flux of K^+ through a pore, formed by four monomers. It was the first K^+ channel to be characterized and due to the high degree of conservation of the central pore, KcsA has become an extensively studied subject for the research of structural components, gating mechanisms and dynamics of potassium channels.[10] KcsA consists of four identical subunits, forming a tetrameric pore complex. One subunit consists of two transmembrane helices TM1 and TM2 that include the cytoplasmic activation gate, the pore helix, the pore mouth, and the selectivity filter (Figure 1A).[10]

Ion flux is regulated by an interplay of the cytosolic activation gate and the extracellular C-type inactivation gate known as selectivity filter.[11,12] The selectivity filter contains the highly conserved signature sequence TVGYG and their backbone carbonyls, together with the sidechain of the threonine, form the four potassium coordination sites S0-S4 (Figure 1B).[11] Gating at the selectivity filter is modulated by a hydrogen-bond and water network behind the filter, which determines its stabilization in the conductive or C-type inactivated state. Key residue E71, commonly replaced by valine or isoleucine in eukaryotes, is at the center of this network, coordinating the backbone of Y78 and the W67 as well as the D80 sidechains (Figure 1B).[11,13] W67 and D80 are highly conserved in K^+ channels, while E71 is commonly replaced by valine or isoleucine in eukaryotes (Figure 1C). Not only the selectivity filter, but also the pore setup is structurally conserved in K^+ channels. Studies have shown that the pore structure of KcsA is highly similar to (eukaryotic) voltage-gated Kv channels, a group that has a voltage sensor which is formed by four additional α-helical transmembrane segments, such as members from the *Shaker* family or the KvAP K^+ channel.[14] That, together with the comparable easy expression and handling, makes KcsA an ideal model to investigate gating of K^+ at the selectivity filter. Single-channel current measurements have shown that WT KcsA displays three different, stochastically shifting gating modes under constant experimental conditions.[15] Substitutions of residue E71 lock the channel in one of the three gating modes: The mutant E71A represents the high-open probability mode with long mean open times of about 100 ms. The eukaryotic-like E71I mutant locks the channel into a low-open probability mode with intermediate mean open times (~10ms). The third gating mode, represented by E71Q KcsA, displays a high-frequency flicker mode with very short open times of less than 1 ms.[15]Curiously enough, crystallographic studies of these mutants showed very similar crystal structures for all three mutants in comparison to WT KcsA (RMSD > 0.25 Å), raising the question how such similar structures can display such different gating behaviour (Figure 1D).[15,16]

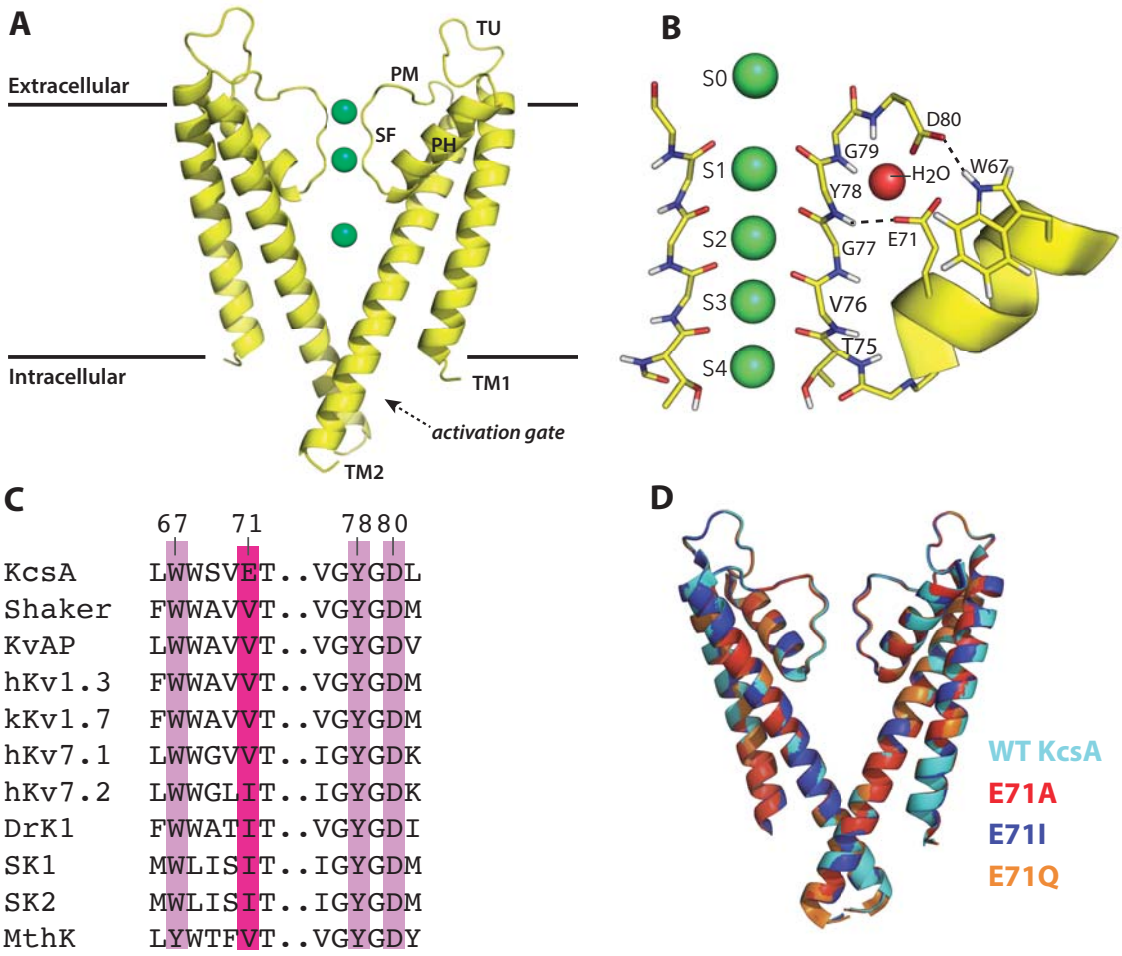

Figure 1. The pore setup is highly conserved in K^+ channels. A) Structure of a KcsA in the closed conductive state (PDB ID: 1K4C). Two monomers are shown in yellow. K^+ ions are shown as green spheres. TM = transmembrane helix, TU = turret loop, PH = pore helix, SF = selectivity filter, PM = pore mouth. B) Zoom into the crystal structure (1K4C). The selectivity filter is regulated by a hydrogen bond and water network with the triad W67-E71-D80 at the center. The highly conserved signature sequence TVGYG is forming the five K^+ coordination sites (S0-S4). C) Residues W67, Y78 and D80 are highly conserved, while E71I is usually replaced in eukaryotic K^+ channels. D) Overlay of the crystal structures of WT KcsA (1K4C)[11], E71A (1ZWI)[16], E71I (3OR7)[49] and E71Q (3OR6) [49] show very high similarity (RMSD < 0.25 Å).

This so-called modal gating behaviour is believed to be a widespread regulatory mechanism not only of potassium channels, but also many other ion channels, such as sodium or calcium channels.[17,18] The underlying mechanisms, however, are still poorly understood.

In this study, modern ^{1}H-detected ssNMR in native-like membranes and at physiological temperatures is used to compare the selectivity filter in WT KcsA and the three mutant channels (E71A, E71I, E71Q) that are best representative of modal gating and to elucidate the molecular determinants of modal gating shifts in K^+ channels.

4 Materials & Methods

4.1 Sample Preparation

Uniformly [^{13}C,^{15}N]-labelled inversely Fractionally Deuterated WT KcsA and E71X mutant channels (E71A, E71I and E71Q) were expressed in *Escherichia coli* M15 cells using standard H_2O-based M9 minimal medium supplemented with 0.5 g/L $^{15}NH4Cl$ and 2 g/L D-glucose-$^{13}C6$-d7.[19] The cells were lysed in a French Press (4 passages, 12,000 psi) and solubilized in detergent (n-Decyl-β-D-Maltopyranoside, Anatrace). The His-tagged protein was extracted and purified as described previously.[20] The purification conditions were slightly changed and the imidazole concentration increased to 50 mM and 70 mM in the binding buffer and washing buffer, respectively, to guarantee highest purity of the samples. Liposome reconstitution was performed using *E.coli* polar lipids (Avanti) at a 1:100 protein:lipid molar ratio using polystyrene beads (Bio-Beads SM-2).[20] Reconstituted samples were suspended in fully protonated phosphate buffer (pH 7.4, 100 mM K^+) in which the channel is in the closed-condutive state.[21] All samples were packed in 1.3 mm ssNMR rotors (Bruker) to allow high magic angle spinning (MAS) frequencies.

4.2 Solid-State NMR Spectroscopy

4.2.1 Spectral assignments

A fully protonated buffer (pH 7.4, 100 mM K^+) was used in order to observe the entire channel in the ^1H-detected ssNMR experiments. To assign the backbone chemical shifts of the E71A mutant, four dipolar-based three-dimensional (3D) ^1H-detected ssNMR experiments (CANH, CONH, CAcoNH, COcaNH) were conducted at 800 MHz (^1H- frequency) using 60 kHz MAS frequency and a real temperature of approximately 305 K. The E71A KcsA assignments were transferred to the E71I and E71Q mutants and confirmed by two 3D experiments (CANH, CONH). 2D ^{13}C-^{13}C PARISxy[22] (N = 1⁄2, m=1) experiments for side chain chemical shift assignments were performed at 700 MHz using 42 kHz MAS and a ^{13}C-^{13}C mixing time of 110 ms.

4.2.2 ^{15}N T_{1rho} relaxation Studies

^{15}N T_{1rho} relaxation experiments were performed as descripted previously for the water-inaccessible part of KcsA and measured at 700 MHz and 58 kHz MAS.[19] For WT KcsA, the E71A mutant, and the E71I mutant channel, ^1H-detected 2D experiments were used together with relaxation increments of $\tau = 0$ (=4 µs), 5, 10, 20, 40 and 80 ms. For the much faster relaxing flicker E71Q channel, we used increments of $\tau = 0$ (=4 µs), 5, 10, 20, 40 and 60 ms. All spectra were processed in the same way and

the relative peak intensities (in reference to the intensity at τ = 0 ms) were analyzed in GraphPad Prism version 7.0a for Mac OS X (Graphpad Software, www.graphpad.com). T_{1rho} was estimated from

$$i = e^{(\frac{-\tau}{T_{1rho}})}$$

with i = relative peak intensity, τ = duration of relaxation increment, a starting value of T_{1rho} = 50 and T_{1rho} had to fulfill the condition $T_{1rho} > 0$. R_{1rho} was calculated as

$$R_{1rho} = \frac{1}{T_{1rho}} \ .$$

The standard error (SE) from the T_{1rho} fitting was used to calculate a relative SE for the error bars. This relative SE was calculated as

$$rel.SE = R_{1rho} * \frac{SE}{T_{1rho}} \ .$$

4.2.3 ^{15}N T_1 relaxation Studies

^{15}N T1 measurements were performed at 950 MHz and 60 kHz MAS using relaxation elements of 0, 2, 4, 10, and 20 s. The W67 side chain is spectrally separate in E71A and E71I (Supplementary Figure 1A-C) and could be analyzed in a series of ^{1}H-detected 1D experiments at 950 MHz.

4.2.4 Proton/Deuterium ($^{1}H/^{2}D$) Exchange Experiments

Proton/deuterium (H/D) exchange 2D NH ssNMR experiments were performed at 800 MHz and 60 kHz MAS. KcsA samples were measured in fully protonated buffer and fully deuterated buffer (both pH 7.4, 100 mM K^+) and deuterated ion channels were incubated for a total of two days prior to the measurement. Signal intensities from 2D NH spectra of all resolved peaks were normalized to the water-inaccessible residues S69 and V70 that are not subjected to H/D exchange.[23]

5 Results & Discussion

5.1 Solid-State NMR chemical shift assignments of the WT channel and E71A, E71I and E71Q KcsA

The ^{1}H, ^{13}C, and ^{15}N ssNMR chemical shifts of the WT channel and the mutants (E71A, E71I, E71Q) in the open-inactivated state (see 4.1) were assigned, starting with a set of four dipolar-based three-dimensional (3D) ^{1}H-detected ssNMR experiments (CANH, CONH, CAcoNH, COcaNH) and a 2D ^{13}C-^{13}C correlation (PARIS) ssNMR experiment to assign backbone chemical shifts of WT KcsA and the E71A mutant (Figure 2A, Supplementary Figure 1 &Supplementary Figure 2). The high spectral quality allowed to almost fully assign residues L41-W87, which include the complete selectivity filter and pore helix, the pore loop, larger part of the outer transmembrane helix (TM1), and a few residues of the inner transmembrane helix (TM2) (Figure 2A). Due to enhanced molecular mobility, the cytoplasmic domain (F125-R160) and the membrane-associated M0 helix (M1-H20) were not detectable in the dipolar-based ssNMR experiments at 300-310 K. The ^{15}N-^{1}H and ^{13}C-^{13}C 2D spectra of the mutant channels (E71A, E71I, E71Q) superimpose well with WT KcsA and each other, confirming the globally conserved fold of the mutant channels. This also allowed to transfer chemical shift assignments to the mutants E71I and E71Q, which then, were confirmed by a reduced set of 3D and 2D ssNMR experiments (CONH, CaNH, ^{13}C-^{13}C PARIS) (Supplementary Figure 1). These assignments were forming the basis for further experiments and analysis.

5.2 E71X substitutions cause stark chemical shift perturbations in the selectivity filter

Chemical shifts are very reliable reporters for the local environment of molecules thus presenting an excellent measurement to monitor the conformation of proteins. Comparing the chemical shifts of the mutant channels to WT KcsA can provide critical information about conformational changes that originate from the substitution of E71 in KcsA and chemical shift differences have been already previously used to identify functional features of the selectivity filter in KcsA.[24]

Intriguingly, stark ^{1}H, ^{15}N and ^{13}C chemical shift perturbations (CSPs) can be observed in all three mutants, especially in the upper part of the selectivity filter and parts of the pore mouth (Figure 2B), which is surprising, considering the very high similarity (RMSD < 0.25 Å) that was observed in the crystal structures of the three mutant channels and WT KcsA.[15,16]

E71A shows strongest combined HN-CSPs for residues Y78 (~2 ppm) and D80 (~1 ppm) relative to WT KcsA. The same can be observed for the ^{13}Ca chemical shifts, that also show maximal CSPs for Y78 and D80 (Figure 2B). Furthermore, the W67 sidechain shows a strong HN –CSP (~0.5 ppm).

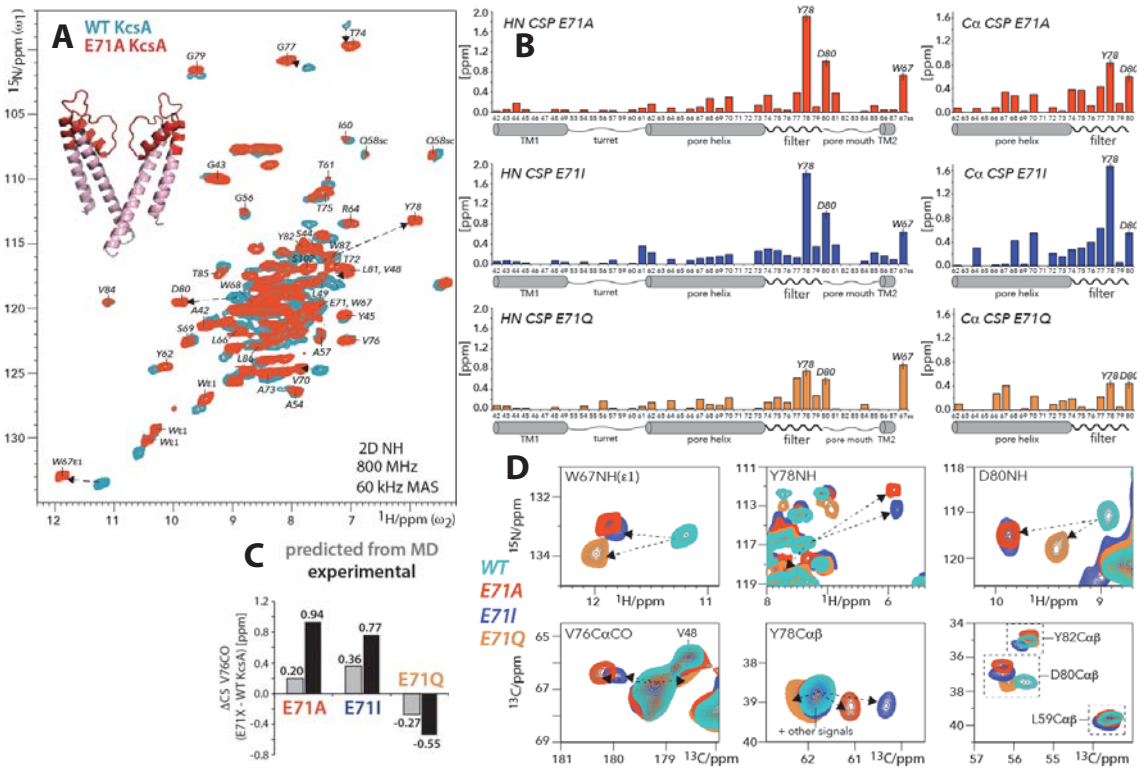

Figure 2. E71X point-mutations cause large conformational changes in the KcsA selectivity filter. A) 2D NH ssNMR spectra of WT KcsA (cyan) and mutant E71A (red) acquired in membranes. Arrows indicate major signal shifts of key residues. Residues L41-W87 are annotated in the E71A spectrum and highlighted in red on the X-ray structure. B) Chemical shift perturbations (CSPs) of E71A (red), E71I (blue), and E71Q (orange) in reference to WT KcsA. (*left*) Combined HN CSPs of amino-protons and backbone-nitrogens and (*right*) Cα CSPs. The strongest NH CSPs in E71A are highlighted in Figure A. C) Comparison of V76CO CSPs derived from experiments (black bars) and back-calculated[28] from MD simulations (grey bars). D) 2D NH (upper panel) and 2D CC spectra (lower) showing large CSPs of key residues W67, V76, Y78, and D80 in E71A (red), E71I (blue), and E71Q (orange) relative to WT KcsA (cyan).

The HN CSP pattern of the key residues W67, Y78 and D80 in E71I KcsA is strikingly similar to the one of the E71A mutant. However, the Ca-CSP of Y78 (~1.7 ppm) is much larger than in E71A KcsA, indicating a structural difference to E71A (Figure 2D).

These three residues, together with E71 are heavily involved in the hydrogen-bond network behind the selectivity filter (Figure 1B), indicating that the substitution of E71 causes conformational changes in the upper selectivity filter and pore mouth that have not been observed in the crystal structures.

The CSPs in E71A and E71I indicate the loss of the X71-D80 interaction which is described as a critical "molecular spring" controlling the stability of the selectivity filter (Figure 3A & B).[13] E71Q KcsA shows the smallest CSPs for these residues in comparison to the other mutants, suggesting that the glutamine mimics some of the hydrogen-bonds by glutamic acid, enabling a comparable interaction to

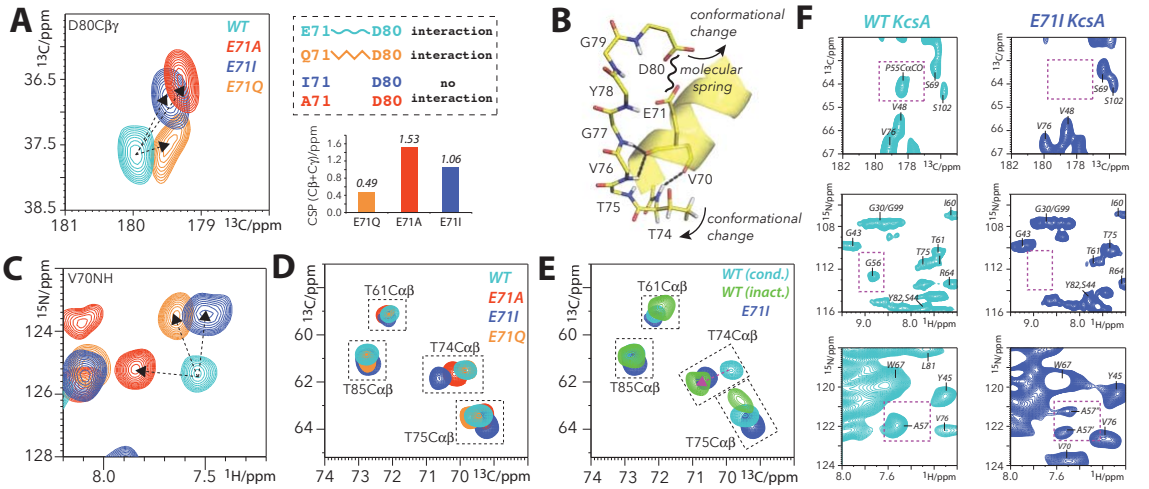

Figure 3. Loss of the E71-D80 interaction causes extended rearrangements behind the filter. A) (*left*) Zoom into 2D CC ssNMR spectra of WT KcsA (cyan), E71A (red), E71I (blue), and E71Q (orange) showing the D80 side chain CSP. (*right*) E71Q mimics the E71 – D80 interaction, which is lost in E71A and E71I. The D80 side chain CSPs are large in E71A and E71I, while they are small in E71Q. B) Structural representation (1K4C) of the stabilisation of filter residues T74-G77 by hydrogen bonds with V70 and E71 of the pore helix. C) Overlay of 2D NH spectra showing a strong CSP for V70 of the pore helix. D) Overlay of 2D CC spectra, showing CSPs of the functionally critical T74 side chain in E71X mutants. E) The large T74 CSP in E71I (pH 7.4, 100 mM K+) is reminiscent of the inactivated filter in WT KcsA (pH 4, 0 mM K+). F) The E71I turret is disordered, which causes signals to disappear or split. Spectral zooms are show for WT KcsA (cyan) and E71I (blue).

D80 as in WT KcsA. Furthermore, in E71Q KcsA, Y78 is also way less perturbed in reference to the WT, supporting the hypothesis that Q71 maintains the interactions to Y78 and D80 (Figure 3A & B). In addition, V70 which is directly next to the X71, also shows strong CSPs, indicating conformational changes at lower part of the pore helix and selectivity filter (Figure 3B & C).

E71 KcsA also shows a clear T74 Ca-CSPs that is very similar to the CSP of T74 observed in WT KcsA after inactivation (pH 4, no K^+; Figure 3D & E), which was demonstrated in previous study as a marker for channel inactivation.[25]

Generally, E71Q shows a similar HN CSP pattern but much less pronounced than the other two mutant channels with maxima at residues Y78 and D80 (both ~0.5 ppm). Also, the direction of some CSPs is different in the flicker mutant E71Q compared to E71A and E71I KcsA (Figure 2D).

All three mutants show strong shifts (~0.5 to 1 ppm) of the V76CO (Supplementary Figure 3), which is forming the S3 K^+ coordination site (Figure 1B), indicating changes in the ion occupancy due to conformational fluctuations. An upfield V76CO chemical shift change is also a known marker for the filter collapse of KcsA due to a low K^+ concentration[26,27] and it is intriguing that E71A as well as E71A show a downfield V76CO, while it shifts upfield in E71Q (Figure 2D).

This is confirmed by chemical shift predictions[28], that were back-calculated from snapshots from MD simulations performed by collaborators (group of Benoît Roux, University of Chicago), who simulated each mutant channel and WT KcsA for 1 µs, providing a total of 400 monomer structures of each channel for the chemical shift predictions. These calculations sampled higher V76CO chemical shifts for E71A and E71I and a decreased chemical shift for the flicker mutant (Figure 2C).

Another noteworthy observation is the disappearing and peak splitting of residues P55, G56 and A57, respectively, in E71I KcsA (Figure 3F).These residues are part of the turret which is known to be a drug binding site[29] and related to gating due to an intrinsic coupling to the hydrogen-bond network behind the selectivity filter.[20] The disappearance and peak splitting of some turret residues strongly indicate long-range effects due to the substitution of E71 by isoleucine.

The key residues W67, Y78 and D80 together with E71 are heavily involved in the hydrogen-bond network behind the selectivity filter (Figure 1B) and large CSPs of these residues were observed in all three mutants, indicating marked conformational dynamics in the upper selectivity filter and pore mouth that demonstrate a structural link to modal gating shifts in KcsA.

5.3 Conformational changes in the selectivity filter modulate the dynamics of the mutant channels

Contradicting historic hypotheses that the selectivity filter is a rigid, domain in K^+ channels to enable fast ion flux and a high selectivity for K^+,[10] recent studies expound that ion selection and ion permeation at the selectivity filter are influenced by dynamical changes[24,30] and that the selectivity filter in WT KcsA is subject to marked molecular motions.[19] Furthermore, molecular dynamics simulations imply that modal gating shifts are related to conformational dynamics.[15]

Protein motions can be measured in T_{1rho} relaxation ssNMR experiments[31], describing a series of relaxation experiments in the presence of a radio-frequency field with an increasing duration of the applied spin-lock field. ^{15}N T_{1rho} relaxation is sensitive to motions in the nano- to millisecond range and dominated by microsecond dynamics and therefore perfectly suitable to investigate domain motions.

To probe these internal dynamics, a series of ^1H-detected 2D ^{15}NH T_{1rho} relaxation experiments were conducted for WT KcsA and the mutant channels (E71A, E71I, E71Q) representing the different gating modes, using relaxation increments of 0, 5, 10, 20, 40, 60/80 ms. The longer the spin-lock duration, the more the signal intensity will decrease, thus giving a decay curve which then can be fitted to estimate T_{1rho} (see 4.2.2; Figure 4B).

Accompanying distinct CSPs, the mutant channels show strikingly different motional landscapes in reference to WT KcsA (Figure 4A). The highest mobility in membrane-embedded domains can be observed in the selectivity filter and pore mouth (~15 ms^{-1} R_{1rho}) with a local maximum at G79,

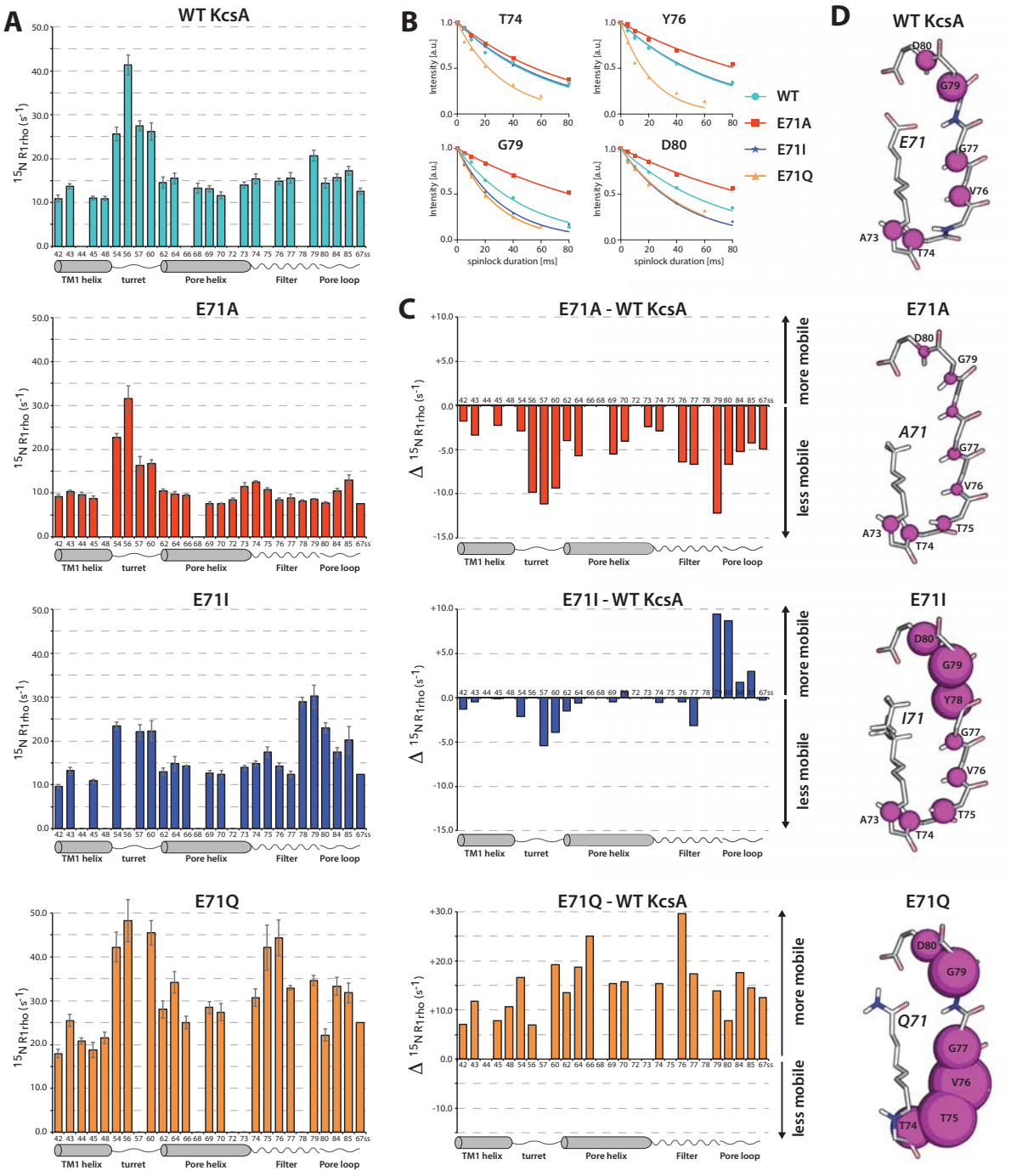

Figure 4. E71X point-mutations strongly change the selectivity filter dynamics. A) 15N rotating-frame ssNMR relaxation rates (R1rho) that report on slow molecular motions in WT KcsA (cyan), E71A (red), E71I (blue), and E71Q (orange) measured at 700 MHz and 58 kHz MAS. B). R1rho signal decay curves for selected filter residues. Symbols mark data points and lines represent best fits. C) Plots of the differences in the dynamics between E71X mutants and WT KcsA. D) Illustration of the site- resolved selectivity filter dynamics. The size of the magenta spheres represents the R1rho relaxation rates.

demonstrating that the selectivity filter is indeed a more flexible domain than historically presumed (Figure 4A). Furthermore, WT KcsA, such as all mutant channels, displays highest dynamics in the

turret loop which is located on the extracellular site and therefore presumably not dynamically restraint by secondary structures or the membrane.

E71A KcsA shows drastically reduced dynamics over the whole protein (Figure 4A). here, residues V76-D80 in the selectivity filter of E71A seem to be immensely rigidified (~8 ms^{-1} R_{1rho}). Also, the pore helix as well as the pore mouth show decreased mobility compared to the WT. The turret is still the most mobile region; however, it is significantly less dynamic than the WT with a difference of ~10 ms^{-1} R_{1rho} (Figure 4C).

The eukaryotic-like E71I mutant showed similar CSP patterns as the E71A channel, however, it has strikingly different dynamics and although the overall motional landscape resembles the WT (Figure 4A), clear local differences can be observed. While the dynamics in the center of the filter around G77 are lower than in the WT, residues in the upper filter and the beginning of the pore mouth (Y78-T85) show clearly enhanced dynamics, again with a maximum at G79 (~30 ms^{-1} R_{1rho}) (Figure 4A). In contrast, the turret seems to be rigidified in E71I, not as much as in the E71A mutant but still displaying -5 ms^{-1} R_{1rho} in reference to the WT, agreeing with the hypothesis that the loss of the E71-D80 interaction causes allosteric effects about 2 nm distal from the mutation site (Figure 4C).

These observations clearly demonstrate, that the strong CSPs in the mutant channels correlate with distinct selectivity filter dynamics on a microsecond timescale.

Intriguingly, the flicker mutant (E71Q) is again clearly distinguishable from the other two mutants. Next to unique CSP patterns, E71Q KcsA is characterized by drastically enhanced overall dynamics (on average +15 ms^{-1} R_{1rho}), explaining the reduced sensitivity in the dipolar-based ssNMR experiments (Figure 4C). Surprisingly, the selectivity filter experiences drastically enhanced dynamics in the flicker channel with ^{15}N R_{1rho} that are comparable to the usually much more mobile turret (Figure 4A).

These results are interesting, as they raise the question if modal gating behaviour[15] correlates with the dynamics in the selectivity filter and the filter entrance: E71A KcsA, displays the lowest dynamics while it has the highest open probability and E71Q a highly dynamic mutant that is characterized by a high-frequency flickering of open and closed states (Figure 4D). The E71I channel, representing the intermediate- or low-open probability mode, shows enhanced dynamics at the filter entrance in reference to the WT.

5.4 The W67-D80 interaction is critical for the stabilization of the selectivity filter

Both, E71A and E71I KcsA display similar CSP patterns and in both cases E71 is substituted by a non-polar residue, thus preventing a hydrogen-bond to Y78. However, E71I shows remarkably different

selectivity filter dynamics, especially in the filter entrance (Figure 4D) and that raises the question asking for the key determinants of these distinct dynamics.

One µs-long molecular dynamics (MD) simulations of WT KcsA and the three mutants (E71A, E71I, E71Q) from collaborators (group of Benoît Roux, University of Chicago) provide a possible explanation for the enhanced dynamics in the selectivity filter entrance of E71I KcsA:

Spectroscopic measurements[27] and electrostatic simulations[32,33] showed that in WT KcsA, E71 possesses an unusually high pK_a which results in protonation of its side-chain. This allows the forming of a hydrogen-bond with D80, therefore locking D80 in a "down" conformation, which enables the

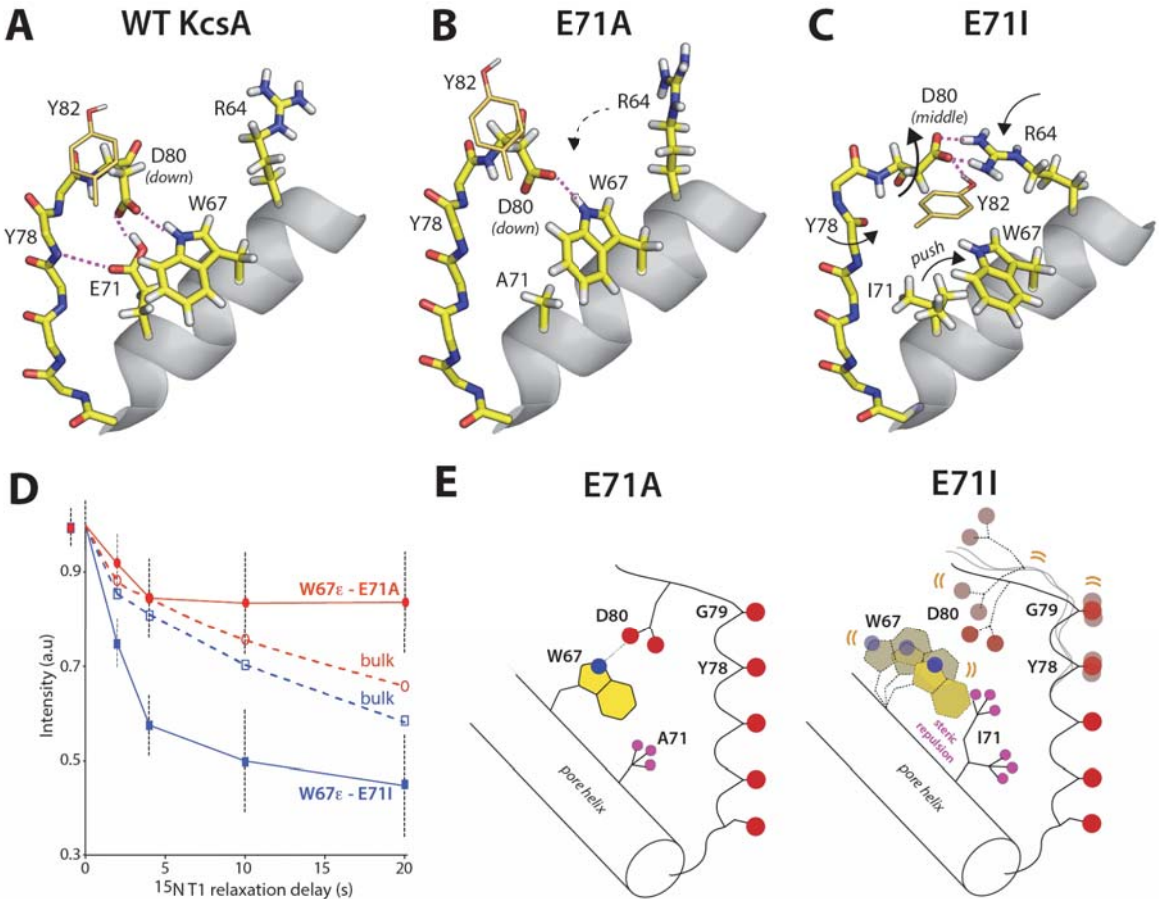

Figure 5. The functionally critical W67 – D80 interaction is destabilized in E71I KcsA. A) WT KcsA MD simulation: The tight interaction with E71 locks the D80 side chain in a *'down'* configuration that enables hydrogen bonding with W67 (snapshot after 270 ns). B) E71A simulation: The *down* conformation prevails, enabling the W67 – D80 interaction, which stabilizes the filter entrance (snapshot after 600 ns). C) E71I simulation: I71 impedes the W67 – D80 interaction which destabilizes the filter entrance. D80 engages in interactions with Y82 (from a neighboring channel subunit) and R64 (snapshot after 600 ns). D) Longitudinal relaxation times (15N T1) that report on fast motion of the W67 side chain for E71A (red circles) and E71I (blue squares), measured at 950 MHz and 60 kHz MAS. The error shows the signal to noise ratio for W67Nε at a given data point. E) (*left*) The W67 – D80 interaction is maintained in E71A. (*right*) I71 hinders the W67 – D80 hydrogen bond, which entails increased dynamics at the pore mouth.

interaction of the indole H of W67 and D80 (Figure 5A) and it was already shown, that W67-D80 interaction is critical for gating and C-type inactivation.[34]

The E71-D80 interaction is lost in the E71A mutant, but the W67-D80 interaction still predominates, thus stabilizing the upper filter (Figure 5B). In E71I KcsA however, the rather large isoleucine side-chain pushes against the W67 side-chain, resulting in a steric hindrance of the W67-D80 interaction (Figure 5C). As compensation, D80 interact more often with two other functionally important residues, namely R64 and Y82[16,35] in E71I and in comparison, this interaction is hardly sampled in the MD simulations of WT KcsA.

This explains the increased dynamics of the filter entrance of the E71I mutant, because the W67-D80 interaction acts as kind of an anchor for this part.

If this is true, increased W67 side-chain mobility should be visible in E71I KcsA, caused by the loss of the stabilizing hydrogen-bond to D80. To confirm this, a series of 1D ^{1}H-detected ^{15}N T_1 relaxation ssNMR experiments were performed for the E71A and E71I channel. T_1 is very sensitive for ps-to-ns motions and therefore better suitable to detect these relatively fast motions of unbound side-chains than T_{1rho}. Indeed, the side-chain of W67 of E71I KcsA shows significantly faster relaxation in reference to the E71A mutant (Figure 5D), which proves enhanced dynamics of the W67 side-chain, caused by the loss of the W67-D80 interaction (Figure 5E).

5.5 H/D exchange experiments reveal fluctuations in the water cavity

A number of crystallographic studies reported the presence of water molecules in a cavity behind the selectivity filter. This buried water was shown to critically influence C-type inactivation and recovery[35–37], and it was proposed that the number of water molecules also affect modal gating[11,15,37]. For E71I and E71A, two water molecules were crystallized behind the selectivity filter, while it could not be determined in E71Q due to insufficient resolution.

It was already shown, that H/D exchange ssNMR experiments[19] can provide well resolved information about the size of the water cavity.[36] Therefore, 2D ^{15}N-^{1}H ssNMR H/D exchange experiments were performed to compare the water exposure of the selectivity filter entrance in WT KcsA and the three mutant channels. For this, samples were measured in fully protonated buffer and fully deuterated buffer (both pH 7.4, 100 mM K^+), in which water accessible protons will exchange with deuterons, resulting in a loss of signal intensity in ^{1}H-detected ssNMR experiments.

Surprisingly, in the selectivity filter (T74-G79) of WT KcsA, G79 is the only residue that exchanges in D_2O while the other filter residues remain un-exchanged (Figure 6A & B) although in the crystal structures it was shown, that a water molecule is next to Y78.[11] This suggests, that the amino-proton of Y78 is protected by a strong hydrogen-bond to the side-chain of E71 (Figure 6D). In the

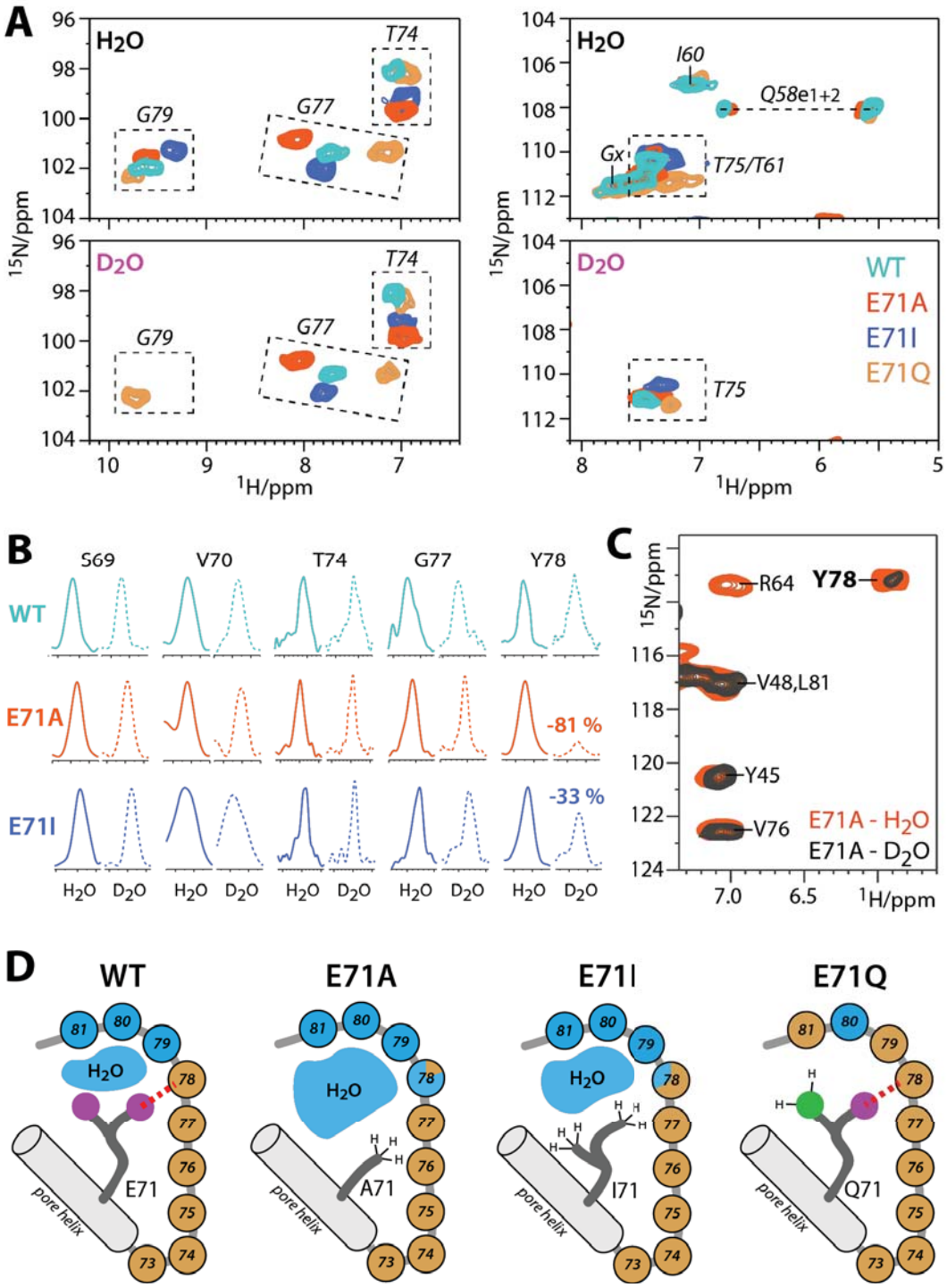

Figure 6. High-resolution analysis of the size of the water cavity behind the filter. A) Zoom into 2D NH ssNMR spectra acquired in (upper panel) protonated and (lower) deuterated buffers of WT KcsA (cyan), E71I (blue), E71A (red), and E71Q (orange). B) Cross-sections from 2D NH spectra of WT KcsA, E71I, and E71A measured in protonated (continuous lines) and deuterated (dashed) buffers. For Y78 in WT KcsA, cross-sections were extracted from 3D CANH experiments to resolve spectral overlap. Signals are normalized (see 00). C) 2D NH spectra of E71A in protonated (red) and deuterated (grey) buffers showing the fast exchange of Y78, implying a larger water cavity. D) Illustrations of the ssNMR-derived water cavity size: in WT KcsA, the cavity is limited to G79-L81, and Y78 is exchange-protected. The cavity widens in E71I, strongly widens in E71A, and is absent in E71Q. Blue and brown spheres represent water-exposed and shielded amino-protons, respectively.

mutants E71A and E71I, however, Y78 shows a decreased intensity, caused by the loss of the protective E71-Y78 interaction (Figure 6B & C). The loss of intensity is lower in E71I (-33 %) and much stronger in E71A (-81 %), implying a wider water cavity in E71A which is made possible by the much smaller size of the alanine side-chain compared to the isoleucine side-chain (Figure 6D). Strikingly, in E71Q neither G79 nor L81 exchange at all, while L81 fully exchanged in WT KcsA and the other two mutants, suggesting that there is no water in the cavity in E71Q (Figure 6A & D).

6 Conclusion

In this study, modern proton-detected solid-state NMR at native-like conditions was used to elucidate the molecular determinants of modal gating shifts in the model K^+ channel KcsA. Mutant channels that represent different gating modes were extensively studied and it was demonstrated that E71X substitutions cause conformational and motional changes in the selectivity filter and pore mouth and resulting in a rearrangement of the hydrogen-bonding and water network behind the filter, which triggers modal gating shifts. Furthermore, the E71X substitutions cause distinct dynamics on a micro-second time-scale which is indicative for domain motions. In addition, the findings on the mutant channel E71I provide a foundation for the understanding of eukaryotic K^+ channels.

7 Outlook: The inactivated state of K^+ channels

The presented results described the molecular determinants of modal gating, emphasizing the conformational and motional dynamics of the selectivity filter which are triggering different gating mode shifts. It is also known that the filter undergoes pronounced conformational changes during inactivation, suggesting that the dynamics of the selectivity filter could also play an important role for the inactivation of the selectivity filter.

The following paragraphs shortly introduce the inactivated state of KcsA and give an outlook on how to study this state by solid-state NMR.

7.1 Introduction

In order to control the ion flux and polarization of membranes, ion channels have to undergo a gating cycle which allows to alternate between open and closed states and conductive or inactivated states, respectively.

There are two distinct inactivation mechanisms known for K^+ channels: Discovered first, N-type inactivation, also described as "ball-and-chain" mechanism, describes a fast occurring auto-inhibitory process of blocking ion conductance on the intracellular site by a conformational change of the amino-terminal region.[38,39] The second mechanism is the so-called C-type inactivation, where the ion conductance is blocked at the filter entrance on the extracellular site of the K^+ channel.[38,40,41]

C-type inactivation is believed to originate from structural rearrangements in the selectivity filter and pore mouth[42] and studies on KcsA suggest that a gradual reorientation of the selectivity filter results in a loss of the S2 and S3 ion coordination sites.[43]

The exact mechanism of C-type inactivation, however, is controversially debated: X-ray studies on KcsA have shown that under low extracellular K^+ conditions the selectivity filter adopts a constricted conformation, where the filter is collapsed and narrowed at G77[11] and it is proposed, that this constricted state represents the C-type inactivated state.[43] Another study has further shown that this state is also adopted under acidic conditions, which are inactivating KcsA at pH 4.[27] Work on a semi-synthetic KcsA channel in which G77 was replaced by a D-alanine, thus prohibiting the constricted conformation, however, argues against that hypothesis because the channel is still able to inactivate.[44] This is supported by two other studies, in which backbone amide-to-ester mutations of the ion coordination sites were used to demonstrate that ion occupancy at the S2 coordination site is required to enable inactivation[45,46], contradicting the constricted-state model which describes a loss of ion occupancy at the S2 site. A recent approach using MD simulations, however, argues against that strict view, by showing that both, the G77D-ala mutant and the mutants with ester-to-amide substitutions at V76, G77, Y78 and G79 indeed, can adopt a constricted-like conformation.

Furthermore, they emphasize the role of the water network behind the selectivity filter which is neglected in the amide-to-ester mutagenesis studies.

This water, located in a cavity behind the selectivity filter, is proven to influence the recovery process from inactivation and thus, stabilizing the inactivated state.[35,36] Furthermore, the hydrogen-bond network and especially the interaction of E71-D80 in KcsA is also proven to be important for the stabilization of the inactivated state[13,34], suggesting that dynamics due to changes in this interaction might come in to play role in the inactivation process.

Studies elucidated the compatibility of KcsA as a model for the inactivation process in eukaryotic voltage-gated Kv channels,[43,47] making it an ideal prototype to investigate K^+ channel inactivation. In our study, modern ^{1}H-detected solid-state NMR (ssNMR) in native-like membranes and at physiological temperatures is used to scrutinize the open-inactivated state in WT KcsA and the eukaryotic Kv channel-like mutant E71V KcsA under acidic and low K^+ conditions.

7.2 Results & Discussion

7.2.1 The inactivated state of WT KcsA under low pH and no K^+ conditions

To assign the ^{1}H, ^{13}C and ^{15}N ssNMR chemical shifts (CS) of WT KcsA in the inactivated state, a 2D ^{15}N-^{1}H ssNMR experiment, a 2D ^{13}C-^{13}C (PARIS) ssNMR experiment and two dipolar-based 3D ^{1}H-detected ssNMR experiments (CONH, CaNH) were performed (see 4.2.1). Two days prior to measuring, the sample buffer was exchanged two times in order to inactivate the channel (10 mM citrate buffer: 150 mM NaCl, no K^+, pH 4, H_20).

The first observation is that the spectral resolution gets notably worse under these conditions (Figure 7A), suggesting a conformational heterogeneity. In reference to the closed-conductive state of WT KcsA (100 mM K^+, pH 7), large ^{15}H-^{1}N chemical shift perturbations (CSPs) can be seen for the open-inactivated state (Figure 7B). Especially the selectivity filter and the beginning of the pore mouth show large CSPs (> 0.5 ppm HN) with a maximum of ~1.5 ppm at D80. HN CSPs of this magnitude generally display conformational changes which are in agreement with the structural changes regarding the collapse of the constricted selectivity filter.[11,43] This can also be seen in the ^{13}C-^{13}C correlation spectrum which shows an upfield shift of the V76CO (~2.9 ppm), indicating changes in the V76-G77 plane that are required for narrowing of the pore at G77 (Figure 7C). The V76 CO is a known marker to determine the collapse of the selectivity filter, as it was reported to shift upfield if the filter collapses in response to K^+ depletion.[26]

In a former ^{13}C-detected study that exclusively observed nitrogen and carbon signals, no significant CSPs could be observed for D80. In our ^{1}H-detected study, we reveal a massive amide ^{1}H CSP resulting in a combined HN CSP of ~1.5 ppm (Figure 7A & B), demonstrating the advantage of ^{1}H-detected ssNMR to study CSPs.

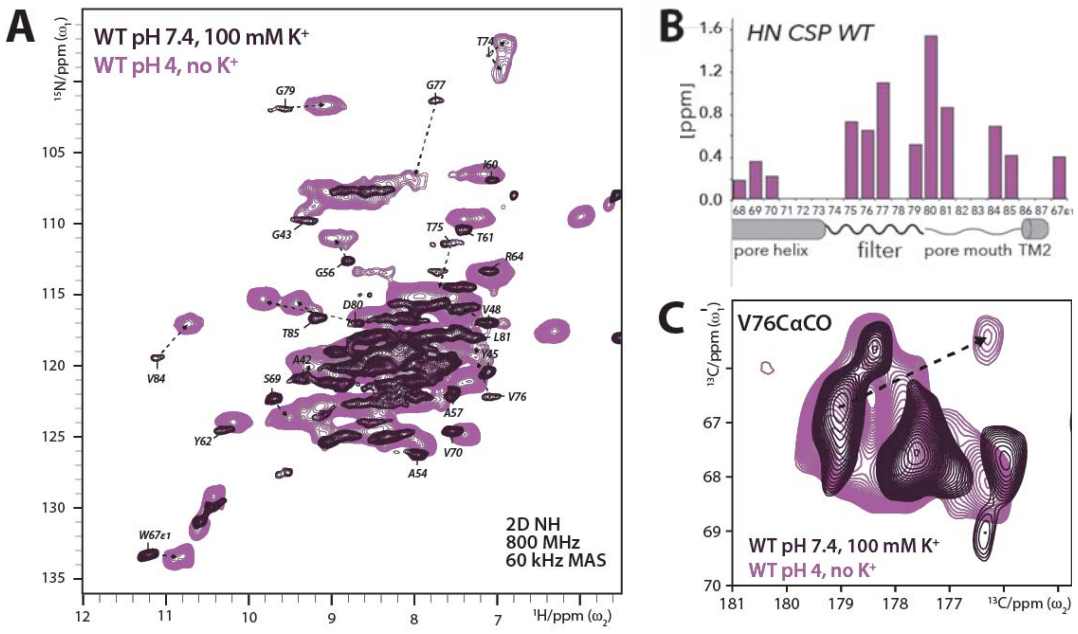

Figure 7. C-type inactivation of KcsA causes marked chemical shift perturbations in the selectivity filter. A) 2D NH ssNMR spectra of WT KcsA in the closed-conductive state at pH 7.4 and 100 mM K^+ (purple) and in the inactivated state at pH 4 and 0 mM K^+ (pink) acquired in membranes. Arrows indicate major signal shifts of key residues. B) Chemical shift perturbations (CSPs) of WT KcsA in the inactivated state (pH 4, no K^+) in reference to the closed-conductive state (pH 7.4, 100 mM K^+). The strongest NH CSPs in E71A are highlighted by arrows in Figure A. C) 2D CC spectra overlay of WT KcsA in the in the closed-conductive state at pH 7.4 and 100 mM K^+ (purple) and in the inactivated state at pH 4 and 0 mM K^+ (pink) showing the CaCO-CSP of V76 due to inactivation.

Another noteworthy observation is the splitting of T74 HN signal in the inactivated state, which is usually an indicator for conformational heterogeneity (Figure 7A). The T74 CSP is a known marker for inactivation[25] but the HN splitting was not described earlier because in comparison to ^{1}H-detected NMR, conventional NMR experiments cannot report on ^{1}H chemical shifts. However, T74 interacts with F103 in the activation gate and F103 was shown to take different rotameric conformations during the inactivation process.[48] These transitional states, could be reflected by different conformations of T74 due to their coupling and thus, leading to a splitting of the signal.

7.2.2 E71V, another eukaryotic-like mutant channel

E71V KcsA is mutated to a valine at position E71, thereby representing eukaryotic Kv channels in which E71 is commonly replaced by an isoleucine or valine (Figure 1C). First, *de-novo* ssNMR chemical shift assignments of E71V in the closed-conductive state had to be obtained in order to investigate changes referring to C-type inactivation of the E71V KcsA. To achieve this, a 2D ^{15}N-^{1}H ssNMR experiment, a 2D ^{13}C-^{13}C ssNMR experiment and two dipolar-based 3D ^{1}H-detected ssNMR

experiments (CONH, CaNH) were performed for E71V KcsA in these two states. E71V KcsA was expressed and prepared in the same way as the other channels (see 4.2.1) and resuspended in fully protonated phosphate buffer (100 mM K^+, pH 7.4) or washed two times in sodium citrate buffer (no K^+, pH 4, H_2O) for two days prior to measurements.

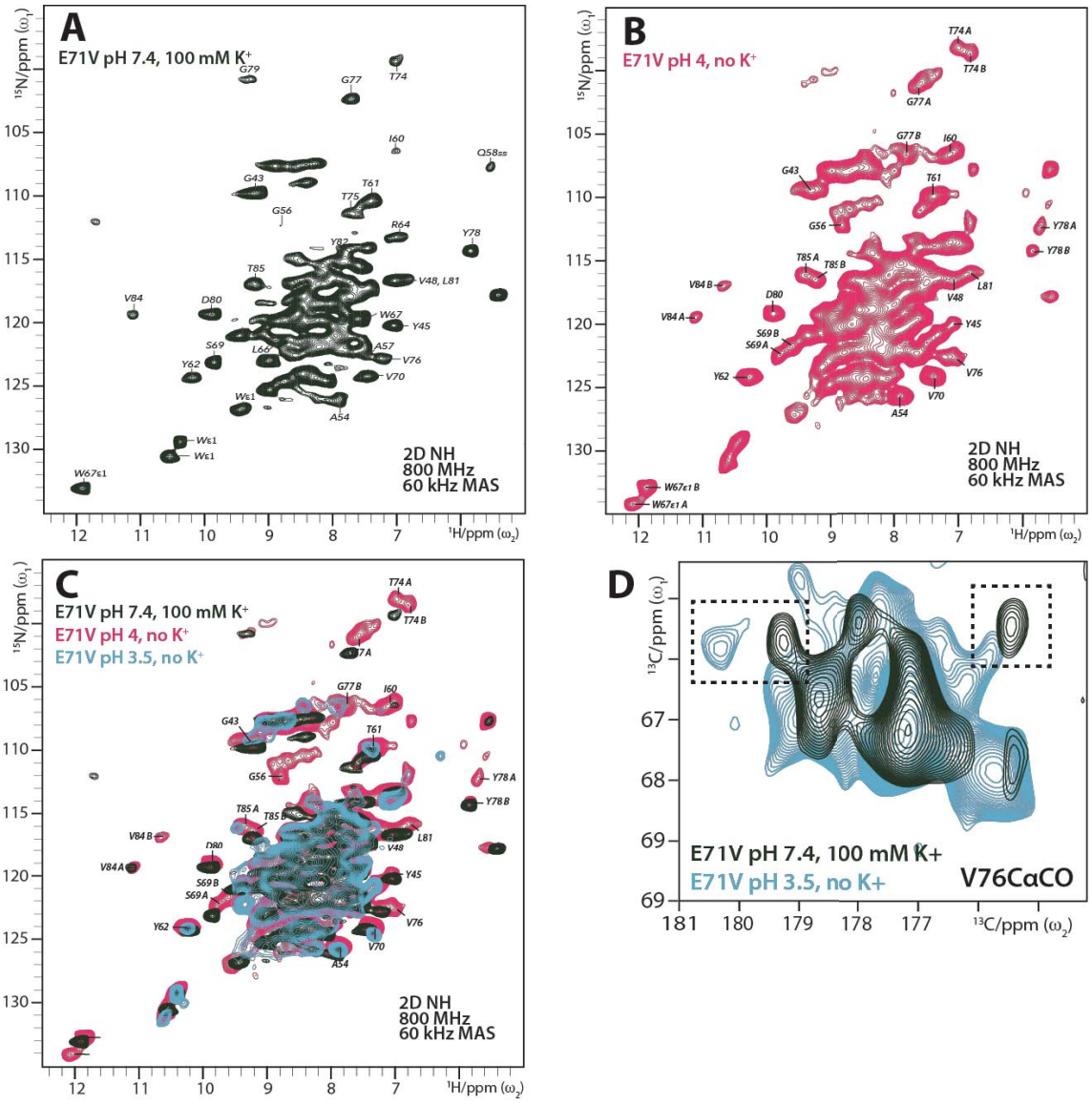

Figure 8. E71V KcsA shows numerous peak splittings due to inactivation. A) 2D NH ssNMR spectrum of E71V KcsA in the closed-conductive state (pH 7.4, 100 mM K^+). Assignments were transferred from the E71I mutant. B) 2D NH ssNMR spectrum of E71V KcsA during inactivation (pH 4, no K^+) shows peak splitting residues in the pore helix (W67ε1, S69), selectivity filter (T74, G77, Y78) and pore mouth (V84, T85) indicating incomplete inactivation. C) Overlay of 2D NH ssNMR spectra of E71V KcsA in the closed-conductive state (pH 7.4, 100 mM K^+; olive) and two inactivation states at pH 4 (magenta) and pH 3.5 (turquoise) without K^+. D) 2D CC spectra overlay of E71V KcsA in the closed-conductive state (pH 7.4, 100 mM K^+; olive) onto E71V in the inactivated state at pH 3.5 and 0 mM K^+ (turquoise) showing two possible states of the V76CO.

The 2D NH spectrum of the E71V mutant in the closed-conductive state superimposes very well with the one of E71I, allowing the transfer of assignments (Figure 8A, Supplementary Figure 4).
Intriguingly, E71V KcsA showed a at least two clearly distinguishable conformations of the outer vestibule at pH 4 (Figure 8B). Numerous ^{15}N-^{1}H peak doublings can be observed for residues in the pore helix (W67ε1, S69), selectivity filter (T74, G77, Y78) and pore mouth (V84, T85), indicating incomplete inactivation and thus displaying more than one state. To test this hypothesis the experiment was repeated at slightly more acidic conditions (sodium citrate buffer, pH 3.5). Indeed, peaks that were representative for the closed-conductive state and present in form of split peaks in the pH 4 spectrum, were gone in the pH 3.5 spectrum, presumably showing full inactivation of the channel (Figure 8C). Based on this, titration experiments could be useful to follow the conformational transitions during the inactivation process. Furthermore, the 2D CC spectra display some ambiguity regarding the CO of V76. Against the expectations that V76CO shifts upfield during inactivation[26], it clearly shifts downfield in E71V at pH 4 and 0 mM K^+. In addition, a second peak shows up around 176 ppm, suggesting a heterogeneity of V76 in the closed-conductive state (Figure 8D).
It is also noteworthy that the spectral quality is lowered again at low pH, agreeing with the observations for WT KcsA and the other two mutants (E71A, E71I) under the same conditions.

7.2.3 Further experiments are required to understand K^+ channel inactivation

To draw specific conclusions regarding the C-type inactivated state of K^+ channels, further experiments are planned and in work. T_{1rho} relaxation ssNMR experiments as presented before, can help to understand the dynamics and stability of the selectivity filter in KcsA in the inactivated state. Studies with the E71A or E71I mutant under these conditions, however, are challenging because the spectral quality is significantly worse in comparison to the same channels in the closed-conductive state. Washing the channel with a deuterated buffer may help to reduce the signal density through exchange of ^{1}H for ^{2}D but first tests gave spectra of insufficient resolution.
It was previously shown, that the water cavity behind the selectivity filter plays an important role in channel inactivation and the recovery from this state.[35–37] $^{1}H/^{2}D$ exchange experiments as previously performed for WT KcsA[36] and the other mutant channels (as presented in 4.2.4) can provide essential information about the eukaryotic-like E71V mutant channel and its water cavity in both, the closed-conductive state and the open-inactivated state.
Furthermore, it would be interesting to record spectra under low K^+ and pH 7 to investigate the closed-inactivated channel and its collapsed selectivity filter.

8 References

1. Wallin, E. & Von Heijne, G. Genome-wide analysis of integral membrane proteins from eubacterial, archaean, and eukaryotic organisms. *Protein Sci.* **7,** 1029–1038 (1998).
2. Hille, B. *Ion channels of excitable membranes*. **507,** (Sinauer Sunderland, MA, 2001).
3. Seddon, A. M., Curnow, P. & Booth, P. J. Membrane proteins, lipids and detergents: not just a soap opera. *Biochim. Biophys. Acta - Biomembr.* **1666,** 105–117 (2004).
4. Helenius, A. & Simons, K. A. I. Solubilization of membranes by detergents. *Biochim. Biophys. Acta (BBA)-Reviews Biomembr.* **415,** 29–79 (1975).
5. Tanford, C. & Reynolds, J. A. Characterization of membrane proteins in detergent solutions. *Biochim. Biophys. Acta - Rev. Biomembr.* **457,** 133–170 (1976).
6. Andersen, O. S. & Koeppe, R. E. Bilayer Thickness and Membrane Protein Function: An Energetic Perspective. *Annu. Rev. Biophys. Biomol. Struct.* **36,** 107–130 (2007).
7. Phillips, R., Ursell, T., Wiggins, P. & Sens, P. Emerging roles for lipids in shaping membrane-protein function. *Nature* **459,** 379 (2009).
8. Callaway, E. The revolution will not be crystallized: a new method sweeps through structural biology. *Nat. News* **525,** 172 (2015).
9. Henzler-Wildman, K. & Kern, D. Dynamic personalities of proteins. *Nature* **450,** 964 (2007).
10. Doyle, D. A. *et al.* The Structure of the Potassium Channel: Molecular Basis of K+Conduction and Selectivity. *Science (80-.).* **280,** 69 LP-77 (1998).
11. Zhou, Y., Morais-Cabral, J. H., Kaufman, A. & MacKinnon, R. Chemistry of ion coordination and hydration revealed by a K+ channel–Fab complex at 2.0 Å resolution. *Nature* **414,** 43 (2001).
12. Yellen, G. The moving parts of voltage-gated ion channels. *Q. Rev. Biophys.* **31,** 239–295 (1998).
13. Cordero-Morales, J. F. *et al.* Molecular driving forces determining potassium channel slow inactivation. *Nat. Struct. &Amp; Mol. Biol.* **14,** 1062 (2007).
14. Long, S. B., Campbell, E. B. & MacKinnon, R. Crystal Structure of a Mammalian Voltage-Dependent Shaker Family K+ Channel. *Science (80-.).* **309,** 897 LP-903 (2005).
15. Chakrapani, S. *et al.* On The Structural Basis of Modal Gating Behavior in K(+) Channels. *Nat. Struct. Mol. Biol.* **18,** 67–74 (2011).
16. Cordero-Morales, J. F. *et al.* Molecular determinants of gating at the potassium-channel selectivity filter. *Nat. Struct. &Amp; Mol. Biol.* **13,** 311 (2006).
17. Alzheimer, C., Schwindt, P. C. & Crill, W. E. Modal gating of Na+ channels as a mechanism of persistent Na+ current in pyramidal neurons from rat and cat sensorimotor cortex. *J. Neurosci.* **13,** 660–673 (1993).
18. Zahradnikova, A. & Zahradnik, I. Description of modal gating of the cardiac calcium release

channel in planar lipid membranes. *Biophys. J.* **69,** 1780–1788 (1995).

19. Medeiros-Silva, J. *et al.* 1H-Detected Solid-State NMR Studies of Water-Inaccessible Proteins In Vitro and In Situ. *Angew. Chemie Int. Ed.* **55,** 13606–13610 (2016).
20. van der Cruijsen, E. A. W. *et al.* Importance of lipid–pore loop interface for potassium channel structure and function. *Proc. Natl. Acad. Sci.* **110,** 13008–13013 (2013).
21. Ader, C. *et al.* A structural link between inactivation and block of a K+channel. *Nat. Struct. Mol. Biol.* **15,** 605–612 (2008).
22. Weingarth, M., Bodenhausen, G. & Tekely, P. Broadband magnetization transfer using moderate radio-frequency fields for NMR with very high static fields and spinning speeds. *Chem. Phys. Lett.* **488,** 10–16 (2010).
23. Medeiros-Silva, J., Jekhmane, S., Baldus, M. & Weingarth, M. Hydrogen bond strength in membrane proteins probed by time-resolved 1H-detected solid-state NMR and MD simulations. *Solid State Nucl. Magn. Reson.* **87,** 80–85 (2017).
24. Baker, K. A., Tzitzilonis, C., Kwiatkowski, W., Choe, S. & Riek, R. Conformational dynamics of the KcsA potassium channel governs gating properties. *Nat. Struct. &Amp; Mol. Biol.* **14,** 1089 (2007).
25. Ader, C. *et al.* Coupling of activation and inactivation gate in a K-channel: potassium and ligand sensitivity. *EMBO J.* **28,** 2825 LP-2834 (2009).
26. Bhate, M. P., Wylie, B. J., Tian, L. & McDermott, A. E. Conformational dynamics in the selectivity filter of KcsA in response to potassium ion concentration. *J. Mol. Biol.* **401,** 155–166 (2010).
27. Bhate, M. P. & McDermott, A. E. Protonation state of E71 in KcsA and its role for channel collapse and inactivation. *Proc. Natl. Acad. Sci.* (2012).
28. Shen, Y. & Bax, A. SPARTA+: a modest improvement in empirical NMR chemical shift prediction by means of an artificial neural network. *J. Biomol. NMR* **48,** 13–22 (2010).
29. Lange, A. *et al.* Toxin-induced conformational changes in a potassium channel revealed by solid-state NMR. *Nature* **440,** 959 (2006).
30. Noskov, S. Y., Berneche, S. & Roux, B. Control of ion selectivity in potassium channels by electrostatic and dynamic properties of carbonyl ligands. *Nature* **431,** 830 (2004).
31. Lewandowski, J. R., Sass, H. J., Grzesiek, S., Blackledge, M. & Emsley, L. Site-specific measurement of slow motions in proteins. *J. Am. Chem. Soc.* **133,** 16762–16765 (2011).
32. Ranatunga, K. M., Shrivastava, I. H., Smith, G. R. & Sansom, M. S. P. Side-chain ionization states in a potassium channel. *Biophys. J.* **80,** 1210–1219 (2001).
33. Berneche, S. & Roux, B. The ionization state and the conformation of Glu-71 in the KcsA K+ channel. *Biophys. J.* **82,** 772–780 (2002).
34. Cordero-Morales, J. F., Jogini, V., Chakrapani, S. & Perozo, E. A multipoint hydrogen-bond network underlying KcsA C-type inactivation. *Biophys. J.* **100,** 2387–2393 (2011).

35. Ostmeyer, J., Chakrapani, S., Pan, A. C., Perozo, E. & Roux, B. Recovery from slow inactivation in K+ channels is controlled by water molecules. *Nature* **501,** 121 (2013).
36. Weingarth, M. *et al.* Quantitative Analysis of the Water Occupancy around the Selectivity Filter of a K+ Channel in Different Gating Modes. *J. Am. Chem. Soc.* **136,** 2000–2007 (2014).
37. Cuello, L. G., Cortes, D. M. & Perozo, E. The gating cycle of a K(+) channel at atomic resolution. *Elife* **6,** (2017).
38. Hoshi, T., Zagotta, W. N. & Aldrich, R. W. Biophysical and molecular mechanisms of Shaker potassium channel inactivation. *Science (80-.).* **250,** 533 LP-538 (1990).
39. Demo, S. D. & Yellen, G. The inactivation gate of the Shaker K+ channel behaves like an open-channel blocker. *Neuron* **7,** 743–753 (1991).
40. Panyi, G., Sheng, Z. & Deutsch, C. C-type inactivation of a voltage-gated K+ channel occurs by a cooperative mechanism. *Biophys. J.* **69,** 896–903 (1995).
41. Ogielska, E. M. *et al.* Cooperative subunit interactions in C-type inactivation of K channels. *Biophys. J.* **69,** 2449–2457 (1995).
42. Liu, Y., Jurman, M. E. & Yellen, G. Dynamic rearrangement of the outer mouth of a K+ channel during gating. *Neuron* **16,** 859–867 (1996).
43. Cuello, L. G., Jogini, V., Cortes, D. M. & Perozo, E. Structural mechanism of C-type inactivation in K+ channels. *Nature* **466,** 203 (2010).
44. Devaraneni, P. K. *et al.* Semisynthetic K+ channels show that the constricted conformation of the selectivity filter is not the C-type inactivated state. *Proc. Natl. Acad. Sci.* **110,** 15698–15703 (2013).
45. Matulef, K., Komarov, A. G., Costantino, C. A. & Valiyaveetil, F. I. Using protein backbone mutagenesis to dissect the link between ion occupancy and C-type inactivation in K+ channels. *Proc. Natl. Acad. Sci.* **110,** 17886 LP-17891 (2013).
46. Matulef, K., Annen, A. W., Nix, J. C. & Valiyaveetil, F. I. Individual ion binding sites in the K+ channel play distinct roles in C-type inactivation and in recovery from inactivation. *Structure* **24,** 750–761 (2016).
47. Gao, L., Mi, X., Paajanen, V., Wang, K. & Fan, Z. Activation-coupled inactivation in the bacterial potassium channel KcsA. *Proc. Natl. Acad. Sci. U. S. A.* **102,** 17630 LP-17635 (2005).
48. Cuello, L. G. *et al.* Structural basis for the coupling between activation and inactivation gates in K+ channels. *Nature* **466,** 272 (2010).
49. Chakrapani, S. *et al.* On the structural basis of modal gating behavior in K+ channels. *Nat. Struct. &Amp; Mol. Biol.* **18,** 67 (2010).

9 Supplementary Figures

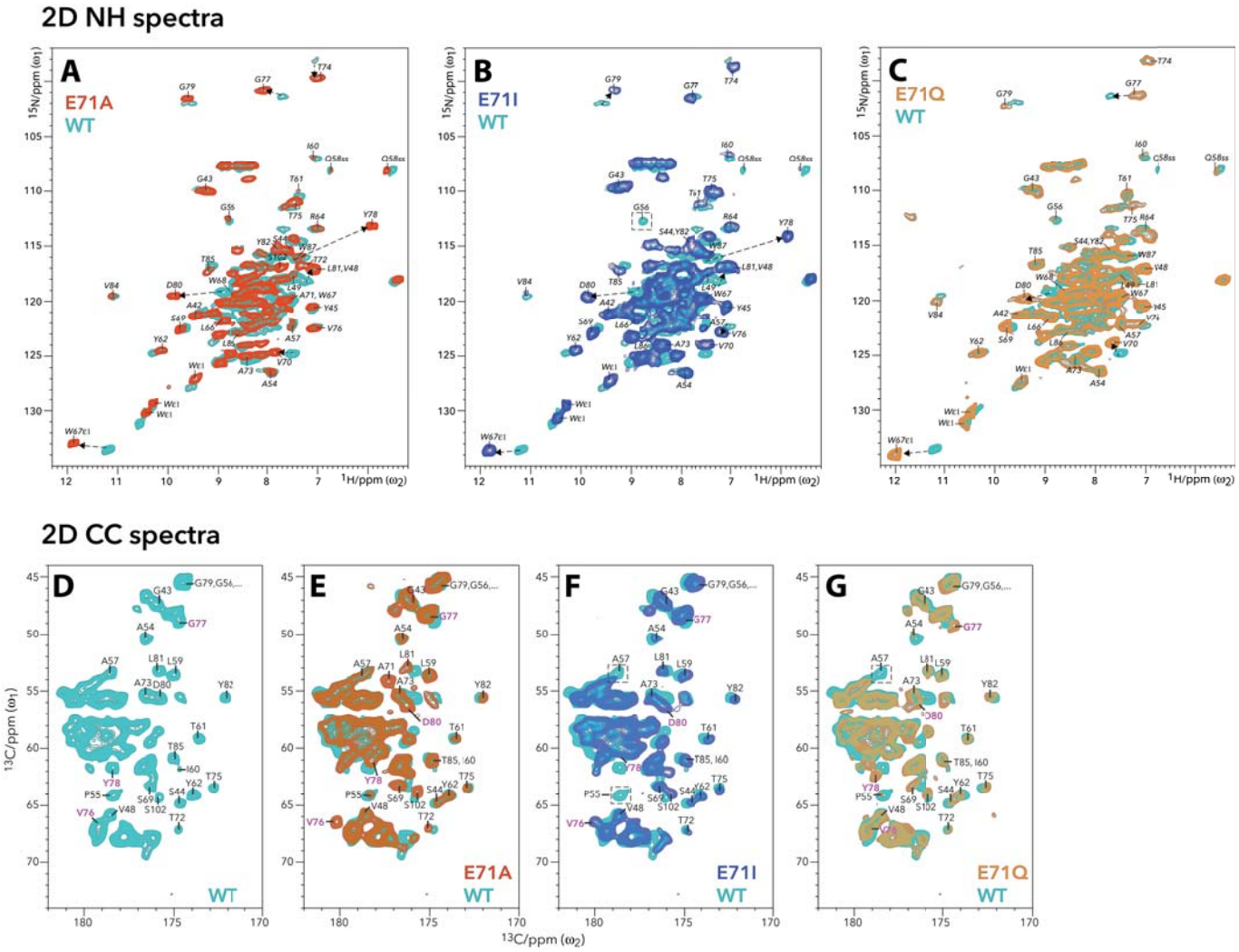

Supplementary Figure 1. Comparison of 2D NH and 2D CC ssNMR spectra of WT KcsA and the E71X mutants. *Upper row:* Overlay of 2D NH spectra of WT KcsA (cyan) onto A) E71A (red), B) E71I (blue), and C) E71Q (orange). *Lower row:* Zoom into the carbonyl-region of 2D CC experiments. D) WT KcsA (cyan), E) E71A (red) and WT KcsA, F) E71I (blue) and WT KcsA, G) E71Q (orange) and WT KcsA. Signals of V76-Y78 and D80 that show larger chemical shift perturbations are highlighted in magenta. Signals of P55-A57 that disappear or split in E71I due to conformational heterogeneity are highlighted in dashed boxes.

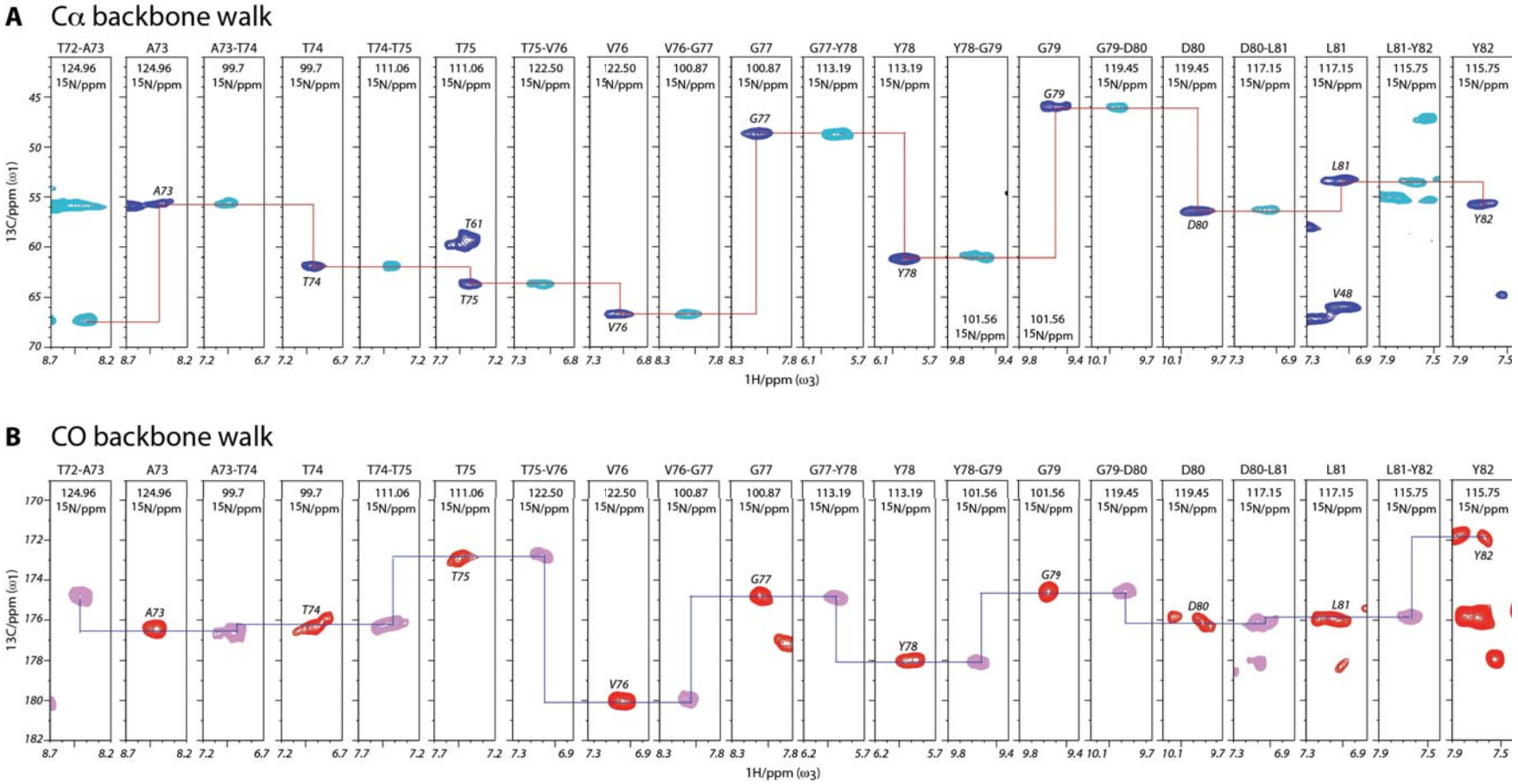

Supplementary Figure 2. Sequential SSNMR assignments with 1H-detected 3D experiments. *Upper panel:* Cα-Cα+1 backbone walk showing full connectivity for residues T72 – Y82 in KcsA mutant E71A. Dark Blue signals show CAH planes from a 3D CANH experiment, cyan CAH planes were taken from a 3D CAcoNH experiment. *Lower panel:* CO-1-CO backbone walk showing full connectivity for residues T72 – Y82 in E71A. Magenta signals show COH planes from a 3D CONH experiment, red COH planes were taken from a 3D COcaNH experiment.

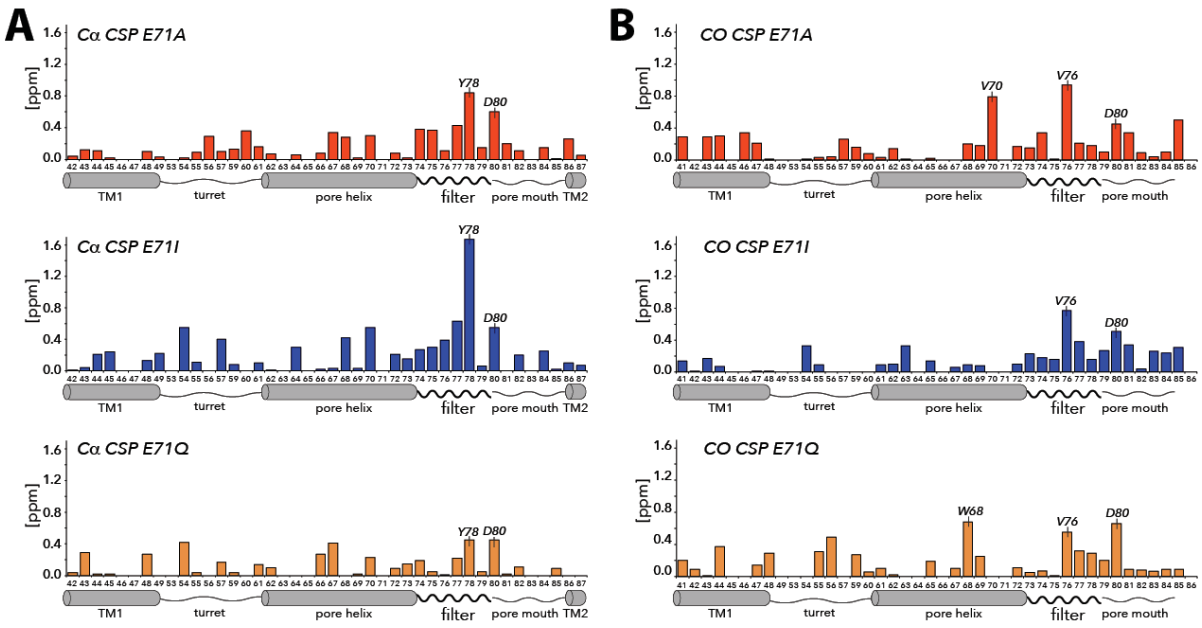

Supplementary Figure 3. Ca and CO ssNMR chemical shift perturbations of the E71X KcsA mutants. *Left panel:* Cα CSPs for E71A (in red), E71I (blue), and E71Q (orange) in reference to WT KcsA. *Right panel:* Corresponding CO CSPs.

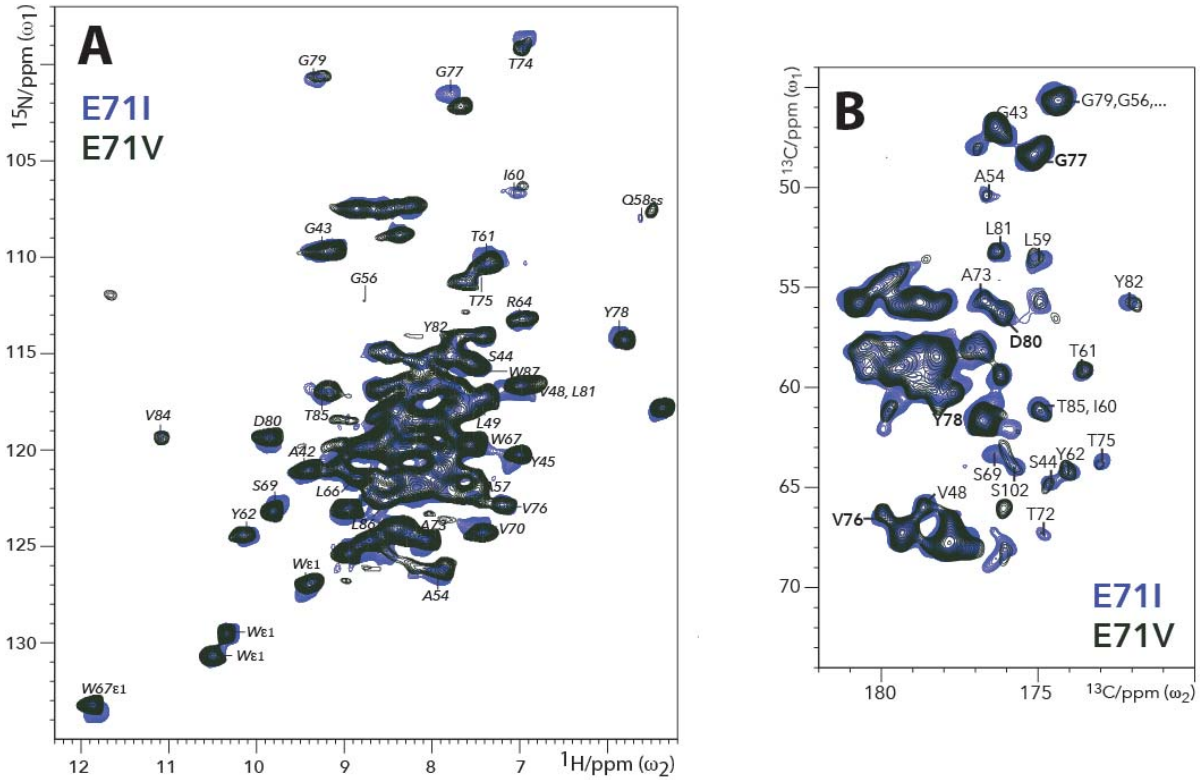

Supplementary Figure 4. Comparison of 2D NH and 2D CC ssNMR spectra of E71I KcsA and E71V. *Left panel:* Overlay of 2D NH spectra of E71V (olive) onto E71I (blue). *Right panel:* Overlay of a zoom into the carbonyl-region of a 2D CC spectra of E71V (olive) onto E71I (blue). Both spectra show the closed-conductive state of KcsA (pH 7.4, 100 mM K^+).